Polymer Journal (2023) 55:591–598
https://doi.org/10.1038/s41428-023-00758-9

ORIGINAL ARTICLE

^{1}H DOSY analysis of high molecular weight acrylamide-based copolymer electrolytes using an inverse-geometry diffusion probe

Kazuya Watanabe[1,2] · Hiroyuki Matsushita[1] · Kyosuke Takamatsu[1] · Koichi Ute[1]

Received: 19 October 2022 / Revised: 23 December 2022 / Accepted: 30 December 2022 / Published online: 2 February 2023

Abstract

Copolymers of [2-(acryloyloxy)ethyl]trimethylammonium chloride (AETAC) and acrylamide (AAm) (AETAC-*co*-AAm) are polyelectrolytes used as flocculants in wastewater purification. Diffusion-ordered two-dimensional NMR spectroscopy (DOSY) experiments for AETAC-*co*-AAm samples with M_w ranging from 1.9 to 3.9 million and a polyacrylamide sample with M_w of 1.3 million were carried out in pure D_2O and in D_2O containing 0.1 or 1 M NaCl using an inverse-geometry diffusion probe system. Projections of the DOSY contour plots onto the diffusion coefficient (D) dimension gave distributions of D for the AETAC and AAm units in the samples. The D values at the maximum point of the distribution (D_p) agreed fairly well with those determined by dynamic light scattering.

Introduction

Copolymers of [2-(acryloyloxy)ethyl]trimethylammonium chloride (AETAC) and acrylamide (AAm) (AETAC-*co*-AAm) (Fig. 1) are important in various industries. For example, they are used as flocculants in paper manufacturing [1, 2], for the enrichment and recovery of minerals from mining [3], and in wastewater treatment [4–6]. Because it comprises polyelectrolytes, AETAC-*co*-AAm provides better flocculation than nonionic polyacrylamide (PAAm) [7–10]. In recent years, more than two kinds of acrylamide-based polymer flocculants have been used because sludge dewatering has become difficult owing to increasing organic matter content in wastewater [11–13].

The properties of AETAC-*co*-AAm in aqueous media have been studied by light scattering and viscometry [4]. The relationships between the weight average molecular weight (M_w), root mean square radius of gyration (R_g in nm) and intrinsic viscosity ([η] in dL/g) were determined for AETAC-*co*-AAm with 30% AETAC: $R_g = 0.033\ M_w^{0.54}$, $[\eta] = 1.05 \times 10^{-4}\ M_w^{0.73}$ (1 M NaCl 25 °C, $4.5 \times 10^5 \le M_w \le 2.7 \times 10^6$). The effect of ionic strength on [η] was also investigated for NaCl concentrations (C_s) between 10^{-2} and 1 mol/L, with a semirigid configuration of the copolymer chains at low C_s values being suggested owing to the absence of a linear relationship between [η] and $C_s^{-1/2}$ [4]. The interaction between AETAC-*co*-AAm and an anionic perfluorinated surfactant was studied by NMR spectroscopy to elucidate the mechanism of flocculation [6]. Full spectral assignment of ^{1}H and ^{13}C resonances was achieved with 1D and 2D experiments. The ^{1}H NMR spectra of AETAC-*co*-AAm with 14% and 23% AETAC in D_2O (1% w/v) showed a higher multiplicity than the corresponding spectra of AETAC-*co*-AAm with 42% and 54% AETAC, and a stiff rod-like structure of the copolymer chains at higher AETAC compositions was suggested. This interpretation was consistent with the ^{13}C NMR spectra of AETAC-*co*-AAm, in which the number of resonances with higher AETAC compositions was smaller than that with lower AETAC compositions [6].

The aim of the present study was to contribute to the characterization of AETAC-*co*-AAm in aqueous media by applying diffusion-ordered two-dimensional NMR spectroscopy (DOSY). DOSY is an NMR method [14–17] that reports diffusion coefficients (D) for individual resonances in NMR spectra. DOSY and the related pulsed field gradient (PFG) NMR diffusometry have been used to determine the

Supplementary information The online version contains supplementary material available at https://doi.org/10.1038/s41428-023-00758-9.

✉ Koichi Ute
ute@tokushima-u.ac.jp

[1] Department of Applied Chemistry, Tokushima University, 2-1 Minami-Josanjima, Tokushima 770-8506, Japan

[2] Kurita Europe GmbH, Industriering 43, Viersen 41751, Germany

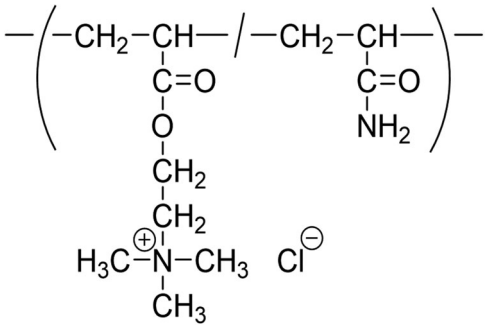

Fig. 1 The chemical structure of AETAC-*co*-AAm

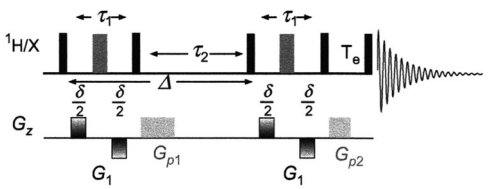

Fig. 2 The *bpp-ste-led* pulse sequence [45]. The encoding gradients of a stimulated echo (*ste*) sequence were applied as symmetrical bipolar pulse pairs (*bpp*) of the total duration, δ. The longitudinal eddy-current delay (*led*) sequence was extended with a delay period, T_e

M_w and molecular weight distribution of synthetic polymers [15, 18–34] and to characterize mixtures of polymers [35–37] and block copolymers [33, 38–43]. A useful tutorial on DOSY experiments for polymers was recently published [44]. Nevertheless, high-molecular-weight AETAC-*co*-AAm in aqueous media is challenging to characterize using DOSY experiments because their D values are as small as $10^{-11.5}$ m^2/s or less and their ^1H resonances suffer from line broadening owing to restricted segmental mobility of the polyelectrolyte chains.

One of the most commonly used pulse sequences for DOSY experiments is the bipolar pulse pair stimulated echo sequence with a longitudinal eddy current delay (*bpp-ste-led*) (Fig. 2) [45]. The observed echo intensity $f(G)$ at a given PFG strength G (in G/cm) is given by the Stejskal–Tanner expression:

$$f(G) = f(G_1)\exp\left(-\frac{2\tau_1}{T_2} - \frac{\tau_2}{T_1}\right)\exp\left[-(\gamma\delta G)^2 D\left(\Delta - \frac{\delta}{3}\right)\right], \quad (1)$$

where G_1 represents the first (the smallest) value of the gradient ramp steps; τ_1, τ_2, δ, and Δ are delays, which are shown in Fig. 2; γ is the magnetogyric ratio of the observed nuclide; and T_1 and T_2 are the longitudinal and transverse relaxation times, respectively. Modern NMR spectrometers are generally equipped with a PFG system (probe and amplifier) generating a maximum G of several tens to 60 G/cm and a maximum δ of several milliseconds. To obtain 5% echo attenuation $f(G)/f(G_1)$, which is required for reliable DOSY experiments, a delay, Δ, of approximately 460 ms (Eq. 1) is required to determine a D of 10^{-11} m^2/s under the following experimental parameters: a maximum G of 60 G/cm and a δ of 5 ms. A larger Δ is necessary as D decreases and as M_w of the solute polymer increases because the relationship between D and M_w roughly obeys $D \propto M_w^{-0.6}$. Applying a large Δ for DOSY experiments of AETAC-*co*-AAm severely reduces the $f(G)$ intensity because T_2 of the copolymer resonances is expected to be less than several tens of milliseconds (see Eq. 1 and Supplemental Material) owing to low segmental mobility, as described above. In our previous studies [37, 46], DOSY experiments of AETAC-*co*-AAm with M_w ranging from 5.1×10^6 to 1.5×10^7 were carried out using a diffusion probe system with a maximum G of 1200 G/cm. The D values determined by DOSY agreed with those determined by dynamic light scattering (DLS). However, the DOSY experiments gave broad distributions of D owing to the low signal-to-noise ratio (S/N) and poor resolution of the spectra. Recently, an inverse-geometry diffusion probe system (with a maximum G of 1800 G/cm) optimized to perform ^1H NMR diffusometry was devised. In contrast to conventional (normal geometry) diffusion probes, which are useful for NMR diffusometry of low γ nuclei, the inverse-geometry diffusion probe is optimized for ^1H DOSY experiments of high molecular weight polymers. For example, Lopez and coworkers reported ^1H NMR diffusometry experiments for polystyrene sulfonates with M_w up to 3.4×10^5 in D_2O using this inverse-geometry diffusion probe [47]. The M_w values of AETAC-*co*-AAm investigated in our present study are larger than those of polystyrene sulfonates by one order of magnitude. This inverse-geometry diffusion probe enabled us to obtain ^1H DOSY spectra with greater resolution than those obtained in our previous studies.

Experimental procedure

Materials

AETAC was purchased from MT Aquapolymer Inc. (Tokyo). AAm and 2,2′-azobis(2-amidinopropane) dihydrochloride (V-50) were purchased from Sigma–Aldrich.

Preparation of polyacrylamide and AETAC-AAm copolymers

Radical polymerization was performed in water at 40 °C for 15 h with V-50 as the initiator. Polyacrylamide (sample A) and AETAC-*co*-AAm (samples B, C, D) with different monomer compositions and molecular weights were synthesized by changing the concentration of V-50 from 0.01 to 1.06 mol% in the monomer mixture. The reactions were

stopped by cooling, and the polymers were isolated by repeated precipitation in acetone. Polyacrylamide and AETAC-*co*-AAm powders were obtained by vacuum drying at room temperature.

NMR measurements

The polyacrylamide and AETAC-*co*-AAm powders were dissolved in D_2O (99.9 atom% D), 0.1 M NaCl in D_2O or 1 M NaCl in D_2O containing 0.05% trimethylsilylpropanoic acid to prepare samples of 0.2 wt% polymer or copolymer. The powders of sample A (or C) and sample D were mixed, and then the solvent was added. These sample solutions were transferred to a sample tube with a 5-mm outer diameter, and the liquid height was adjusted to 30 mm. DOSY measurements were performed using a Bruker AVANCE NEO 400 spectrometer equipped with the Diff BBI probe and the Diff-5-3 program implemented in TopSpin 4.1.0 software. For the measurements of the polymer samples in D_2O containing 1 M NaCl at 30 °C, data were acquired using the *bpp-ste-led* sequence [45] (PULPROG: diffSteBp) with a gradient pulse length (δ) of 3.2 ms (gradient pulse shape: *smsq*), a diffusion delay (Δ) of 10 ms, an eddy current delay (T_e) of 5 ms, and a gradient recovery delay (t_g) of 0.5 µs. The parameters for the measurements under other conditions are given in the figure legends. All experiments were recorded using 128 scans for each gradient strength in 128 linear G lamp steps. The acquisition time was 0.84 s with a relaxation delay of 4.16 s using 8192 data points for the F_2 dimension covering 4850 Hz. The transmitter frequency offset was adjusted to the frequency of the $N(CH_3)_3^+$ resonance. An exponential window with a broadening factor of 3 Hz was applied prior to Fourier transform along the F_2 dimension. Careful phase adjustment and baseline correction were performed. The CONTIN method [48, 49] implemented in the TopSpin 4.1.4 software was adopted for inversion of the Laplace transform along the F_1 dimension.

SEC-MALS measurements

Size exclusion chromatography coupled with multiangle light scattering (SEC–MALS) measurements were performed in 1 M NaCl at 25 °C to determine the M_w, M_w/M_n, and root mean square radius of gyration (R_g) of the polyacrylamide and AETAC-*co*-AAm samples. The powders of these samples were dissolved in 1 M NaCl to give 0.2 wt% solutions. An MALS detector (WYATT DAWN HELEOS-II) and two SEC columns (Shodex OHpak SB-806 M HQ with a maximum porosity of 2 million and OHpak SB-807 HQ with a maximum porosity of 50 million) were used for the analysis. Aqueous NaCl (1 M) was used as the eluent, and the flow rate was 0.6 mL/min. A Wyatt Optilab T-rEx differential refractometer was calibrated using a series of 1 M NaCl solutions of known concentrations [50].

Dynamic light scattering measurements

DLS measurements of the polymer samples were carried out for 0.2 wt% solutions in 1 M NaCl at 30 °C using a Malvern Panalytical Zetasizer Nano ZSP system and a 10-mm polystyrene cell. The powders of polyacrylamide and AETAC-*co*-AAm were dissolved in 1 M NaCl to prepare samples of 0.2 wt% polymer or copolymer. The powders of sample A and sample D were mixed, and then the solvent was added. Inversion of the Laplace transform was conducted using the CONTIN method implemented in Zatasizer software (version 8.02).

Intrinsic viscosity measurements

The [η] of the polymers was measured in 1 M NaCl at 25 °C using a Cannon–Fenske viscometer (size 75). The intrinsic viscosity values were extrapolated from the linear plots of the reduced specific viscosity as a function of concentration [50].

Results and discussion

Table 1 summarizes the average AETAC composition, M_w, M_w/M_n, R_g, and [η] of samples A to D. It should be noted that the [η] values increased with increasing M_w. According to the work of Mabire et al., in a 1 M NaCl solution, [η] is affected by the ionic strength of the solution as well as the composition and M_w of the polymer,

Table 1 Homopolymer of AAm and copolymers of AETAC and AAm prepared by radical polymerization at 40 °C[a]

Sample	AETAC (mol%)		M_w[c]/10^6	M_w/M_n[c]	R_g[c] (nm)	$[\eta]$[d] (dL/g)
	Feed[a]	Copolymer[b]				
A	0	0	1.3	1.6	61	5.4
B	60	59.3	2.1	2.8	87	7.7
C	60	59.4	1.9	2.6	86	7.5
D	80	80.9	3.9	3.1	109	10.1

[a]V-50 was used as the initiator (0.01–1.06 mol% of monomer). The monomer concentration in water was 4.6 mol/L

[b]Determined by ^{1}H NMR in 1 M NaCl in D_2O at 40 °C using the following Eq.:

AETAC (mol%) = Intensity ($N(CH_3)_3$/9)/Intensity ($(CH+CH_2/3)$)

[c]Weight average molecular weight (M_w) and root mean square radius of gyration (R_g) determined by SEC–MALS measurements in 1 M NaCl at 25 °C

[d]Determined in 1 M NaCl at 25 °C

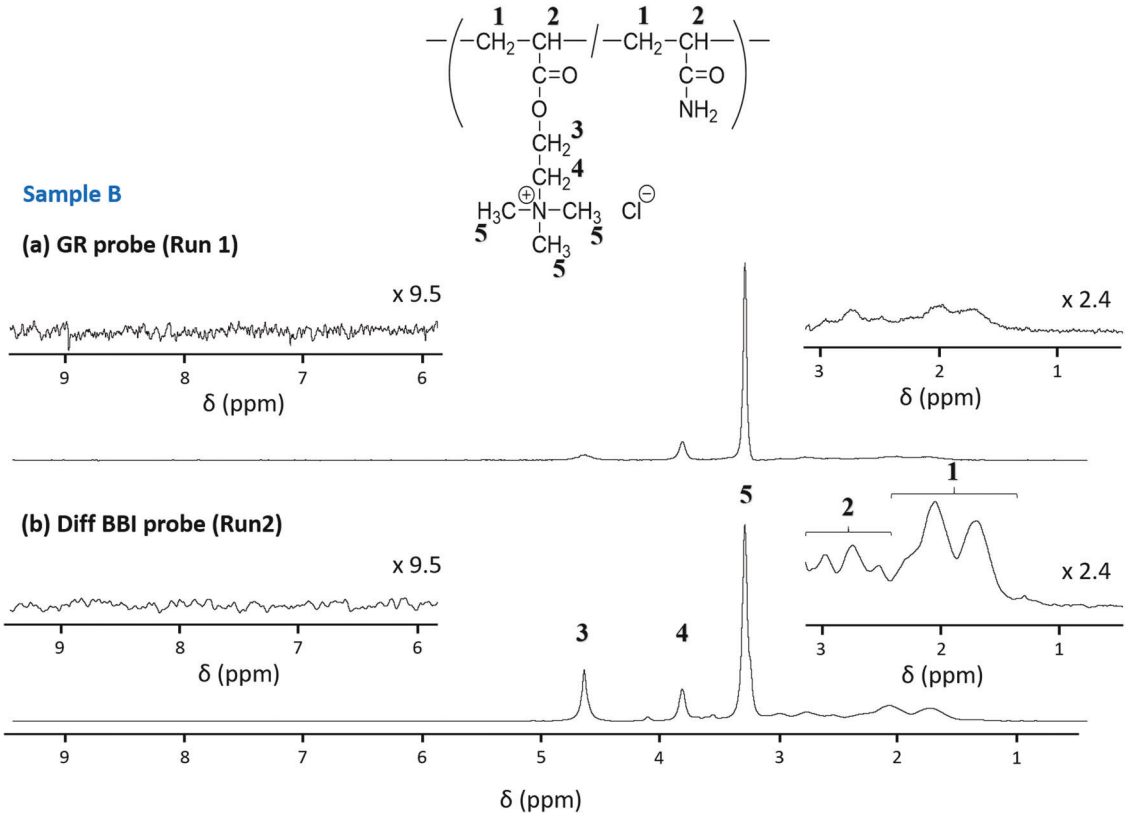

Fig. 3 1D NMR spectra extracted from the DOSY data of sample B in D_2O at 40 °C. The spectra were acquired at the first gradient step, G_1. The DOSY experiments were performed using the GR probe (previous study, Run 1) (**a**) and the Diff BBI probe (present study, Run 2) (**b**). See Table 2 for the parameters of these experiments

and R_g is affected by M_w but not by the composition of AETAC-*co*-AAm [4].

Figure 3b shows the 1D NMR spectrum extracted from the DOSY data of sample B measured in D_2O at 40 °C. The spectrum was acquired at the first gradient step, G_1. The parameters for the DOSY experiment are shown in Table 2 as Run 2. According to the assignments by Proietti et al. [6], the broad resonances at 1.35–2.41 and 2.41–3.04 ppm can be assigned to the CH_2 (**1**) and CH (**2**) groups of the copolymer main chain, respectively. We assigned the strong resonance at 3.24 ppm to the $(CH_3)_3N^+$ group (**5**) and the resonances at 3.77 and 4.59 ppm to the CH_2 groups of the AETAC side chain (**3**, **4**). A comparison of this spectrum with that of Fig. 3a in our previous study [37, 46] (the parameters are shown in Table 2 as Run 1) reveals that the intensities of resonances **1**–**4** were higher than that of resonance **5**. We mainly attribute this increase to the reduction of the diffusion time (Δ) from 100 ms (Run 1) to 10 ms (Run 2), which was made possible by the use of the Diff BBI probe. The T_2 values for resonances **1**–**4** were smaller than that of resonance **5** (see Supplementary Material). Thus, using a large Δ leads to severe loss of the echo intensity for small T_2 resonances (see Eq. 1).

Table 2 Parameters for the DOSY experiments of AETAC-*co*-AAm (sample B) used in our previous studies (Run 1) [37, 46] and in the present study (Run 2)[a]

Run	1	2
Spectrometer	JEOL JNM-ECA	Bruker Avance NEO
Probe	5 mm GR	5 mm Diff BBI
Observed frequency (MHz)	500	400
Δ (ms)	100	10
δ (ms)	2.0	2.5
t_g (μs)	238	0.5
T_e (ms)	50	5
n	32	128
Number of G steps	32	64
Shape of the gradient pulse	square	smooth square
G_1 (G/cm)	100	80
G_{max} (G/cm)	1100	1720
S/N of the $(CH_3)N^+$ resonance[b]	263.7	861.5
S/N of the CH_2 resonance[b]	9.9	47.0

[a]DOSY experiments in D_2O at 40 °C. t_g denotes the gradient recovery time (see Fig. 1 for the other abbreviations of the delay times (Δ, δ, T_e)); n is the number of gradient steps (linear G ramp); and G_1 and G_{max} are the strengths of the minimum (the first) and maximum (the n-th) gradients, respectively

[b]Signal-to-noise ratio for the 1D spectrum obtained at G_1. An exponential apodization function (LB = 3.0 Hz) was applied prior to the Fourier transform along the F_2 dimension. The noise region for the S/N calculations was 6.5–10.0 ppm

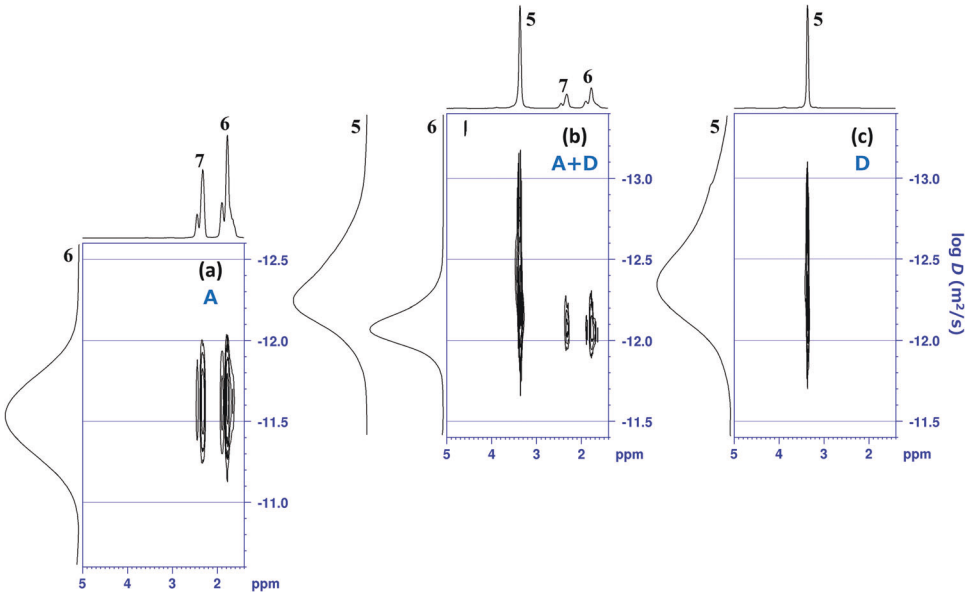

Fig. 4 DOSY-CONTIN contour plots with F_1 (the D dimension) and F_2 (the chemical shift dimension) projections of sample A (**a**), sample D (**c**), and a 1:1 mixture of samples A and D (**b**). The DOSY experiments were performed in D_2O at 40 °C. Sample concentration = 0.2 wt %; $\Delta = 12$ ms; $\delta = 5.4$ ms; number of linear G steps = 64 (**a**) or 128 (**b**, **c**); $G_{64} = 700$ G/cm (**a**); and $G_{128} = 1400$ and 1420 G/cm in (**b**) and (**c**), respectively

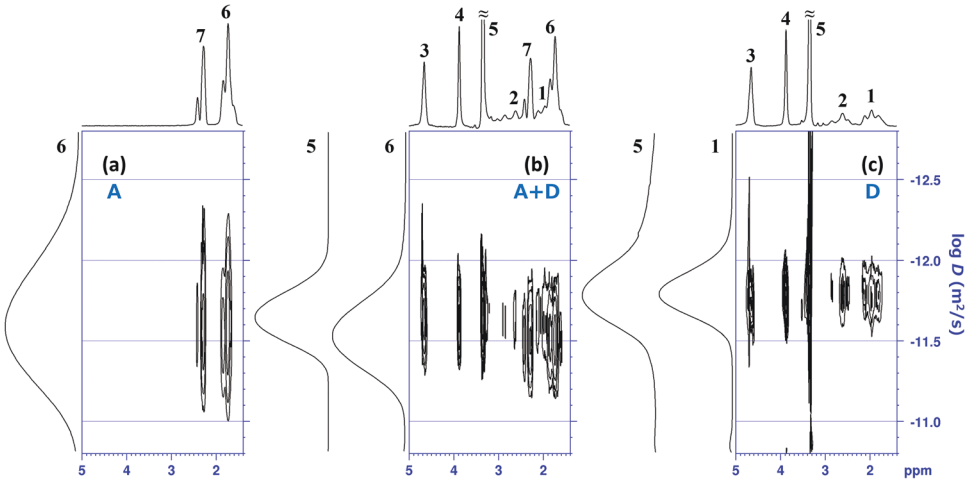

Fig. 5 DOSY-CONTIN contour plots with F_1 and F_2 projections of sample A (**a**), sample D (**c**), and a 1:1 mixture of samples A and D (**b**). The DOSY experiments were performed in 1 M NaCl in D_2O at 30 °C. Sample concentration = 0.2 wt%; $\Delta = 10$ ms; $\delta = 3.4$ ms; number of linear G steps = 128; and $G_{128} = 1100$, 1400, and 1650 G/cm in (**a**–**c**), respectively

Figure 4 shows the DOSY contour plots with F_1 (the D dimension) and F_2 (the chemical shift dimension) projections obtained from the CONTIN analysis of samples A and D and a 1:1 mixture of A and D in D_2O at 40 °C. The plots for sample A (Fig. 4a) show the resonances due to the CH_2 (**6**) and CH (**7**) groups of the polyacrylamide main chain and the log–Gaussian distribution of D with the peak maximum (D_p) at a log D of -11.52 m^2/s. In contrast, almost no resonances other than that due to the $(CH_3)_3N^+$ group (**5**) of the AETAC side chain were observed in the plots for sample D (Fig. 4c). The log D_p was found at -12.33 m^2/s. The plots for the mixture of samples A and D (Fig. 4b) showed resonances **6** and **7** of polyacrylamide and resonance **5** of AETAC-*co*-AAm. The distributions of D for samples A and D were well separated, with log D_p values at -12.09 and -12.27 m^2/s, respectively. Polyacrylamide (sample A) is uncharged and has a flexible chain structure, whereas AETAC-*co*-AAm (sample D) is a polyelectrolyte, which we assume has a relatively expanded chain structure in D_2O owing to electrostatic repulsion between the charged AETAC units. We consider that the expansion of AETAC-*co*-AAm chains reduces the segmental mobility of the main chain and makes T_2 of resonances **1**–**4** very small. Even with a small Δ of 12 ms, which was achieved by the use of the Diff BBI probe, it seems difficult to observe resonances **1**–**4** from DOSY experiments in pure D_2O.

It should be noted that the log D_p for sample A in Fig. 4b (-12.09 m^2/s) was significantly smaller than that in Fig. 4a (-11.52 m^2/s). We attribute the decrease in D_p when sample A was mixed with sample D to the concentration of 0.2 wt% in D_2O far exceeding the overlap concentration (c^*). The individual polymer chains start to overlap as the concentration approaches c^*, which is defined as the concentration at which a given dilute conformation's pervaded volume is equal to the solution concentration [51]. The need to use sufficiently low-concentration samples to determine

the correct D by diffusometry has been noted in the literature [22, 32, 52, 53]. However, DOSY experiments for AETAC-*co*-AAm samples at concentrations below 0.2 wt% were impractical in terms of sensitivity of the spectrometer in the present study.

Figure 5 shows the DOSY contour plots with F_1 and F_2 projections of samples A and D and the mixture of samples A and D in 1 M NaCl in D_2O at 30 °C. In contrast with Fig. 4b, c, resonances **1**–**5** of AETAC-*co*-AAm were observed in Fig. 5b, c, and resonances **6** and **7** of polyacrylamide were observed in Fig. 5a, b. It was reported that the intramolecular electrostatic repulsion between charged segments by $(CH_3)_3N^+$ in AETAC-*co*-AAm is screened by Cl^- and that polymer chain expansion is not appreciable in D_2O solution with salt [9]. As a result, the log D_p for sample D increased markedly to $-11.78\ m^2/s$ (Fig. 5c). The distributions of D for samples A and D in Fig. 5b separated well, with log D_p values at -11.51 and $-11.64\ m^2/s$, respectively. These values agreed reasonably well with those determined by DLS-CONTIN analysis for sample A ($-11.26\ m^2/s$) and sample D ($-11.58\ m^2/s$) in 1 M NaCl in D_2O at 30 °C (Fig. 6). However, we note that the D determined by DLS is a mutual-diffusion coefficient in contrast with the self-diffusion coefficient determined by DOSY. Separations of samples A and D along the diffusion axis determined by DOSY (Fig. 5b) and DLS (Fig. 6) compare unfavorably with the SEC separation, which showed a bimodal distribution of molecular weight corresponding to samples A and D (Fig. 7). We attribute the insufficient separation in the SEC curve for the mixture of samples A and D to overloading of the sample solution in the SEC-MALS instrument.

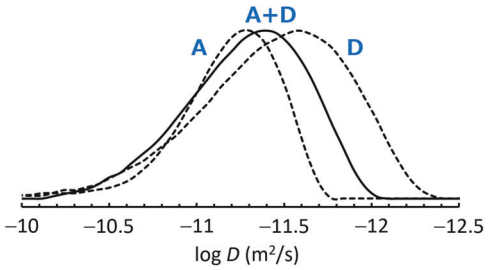

Fig. 6 Distribution of D determined by DLS-CONTIN analysis of sample A, sample D, and a 1:1 mixture of samples A and D in 1M NaCl in D_2O at 30 °C. Sample concentration = 0.2 wt%

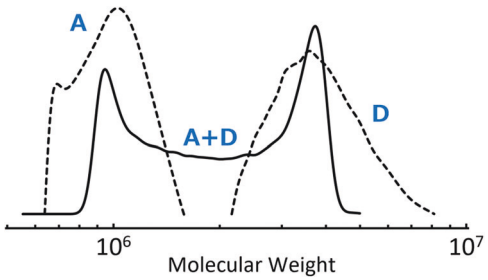

Fig. 7 Molecular weight distributions of sample A, sample D, and a 1:1 mixture of samples A and D measured by SEC–MALS using 1 M NaCl in water as the eluent at 25 °C

Figure 8b shows the DOSY contour plots with F_1 and F_2 projections of a 1:1 mixture of samples C and D in 0.1 M NaCl in D_2O at 30 °C. The M_w of sample D (3.9×10^6) was twice as large as that of sample C (1.9×10^6), and the AETAC composition of sample D (80.9 mol%) was larger than that of sample C (59.4 mol%). However, the F_1 (the diffusion dimension) projection showed no sign of separation or broadening arising from the two copolymers. Thus, it appears difficult to separate the diffusion profiles of these samples by DOSY analysis under the conditions of this study.

Our results demonstrate that the inverse-geometry diffusion probe system is useful for the DOSY-CONTIN analysis of polyelectrolytes with M_w over one million in D_2O

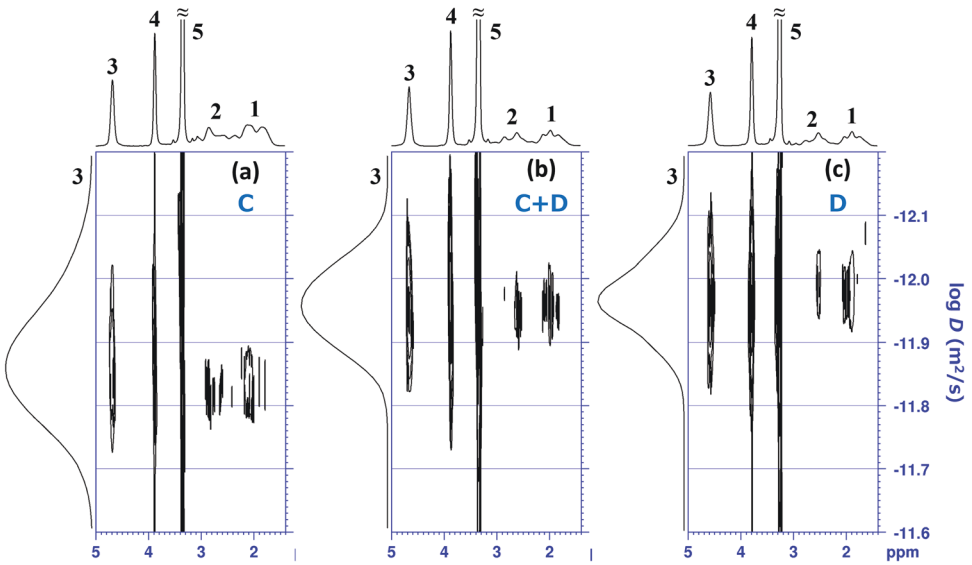

Fig. 8 DOSY-CONTIN contour plots with F_1 and F_2 projections of sample C (**a**), sample D (**c**), and a 1:1 mixture of samples C and D (**b**). The DOSY experiments were performed in 0.1 M NaCl in D_2O at 30 °C. Sample concentration = 0.2 wt %; Δ = 11 ms; δ = 3.8 ms; number of linear G steps = 128; and G_{128} = 1250, 1550, and 1500 G/cm in (**a**–**c**), respectively

containing 0.1 to 1 M salts. This is particularly relevant to the study of sludge solutions. For example, the electrical conductivity of common sludge is approximately the same as that of 0.1 M NaCl aqueous solution (22 μS/m) [54]. Many studies have been conducted to elucidate the mechanism of sludge dehydration using polymer flocculants, although few have focused on the structure of these polymers [55, 56]. We expect that the application of the DOSY-CONTIN method will provide information on the structure and mobility of polymer flocculants in stimulated sludge solutions.

Acknowledgements The Bruker AVANCE NEO 400 spectrometer with the Diff BBI probe was financially supported by the Polymer DOSY Consortium of Tokushima University.

Compliance with ethical standards

Conflict of interest The authors declare no competing interests.

Publisher's note Springer Nature remains neutral with regard to jurisdictional claims in published maps and institutional affiliations.

References

1. Howard GJ, Hudson FL, West J. Water-soluble polymers as retention aids in a model papermaking system. III. Modified polyacrylamides. J Appl Polym Sci. 1977;21:29–43. https://doi.org/10.1002/app.1977.070210103.
2. Pelton RH, Allen LH. The effects of some electrolytes on flocculation with a cationic polyacrylamide. Colloid Polym Sci. 1983;261:485–92. https://doi.org/10.1007/BF01419832.
3. Moody G. The use of polyacrylamides in mineral processing. Minerals Eng. 1992;5:479–92. https://doi.org/10.1016/0892-6875(92)90227-Z.
4. Mabire F, Audebert R, Quivoron C. Synthesis and solution properties of water soluble copolymers based on acrylamide and quaternary ammonium acrylic comonomer. Polymer. 1984;25:1317–22. https://doi.org/10.1016/0032-3861(84)90383-5.
5. Lafuma F, Durand G. 13C NMR spectroscopy of cationic copolymers of acrylamide. Polym Bullet. 1989;21:315–8. https://doi.org/10.1007/BF00955924.
6. Proietti N, Amato ME, Masci G, Segre AL. Polyelectrolyte/surfactant interaction: an NMR characterization. Macromolecules. 2002;35:4365–72. https://doi.org/10.1021/ma012238t.
7. Woo S, Lee JY, Choi W, Moon MH. Characterization of ultrahigh-molecular weight cationic polyacrylamide using frit-inlet asymmetrical flow field-flow fractionation and multi-angle light scattering. J Chromatography A. 2016;1429:304–10. https://doi.org/10.1016/j.chroma.2015.12.027.
8. Wei H, Gao B, Ren J, Li A, Yang H. Coagulation/flocculation in dewatering of sludge: a review. Water Res. 2018;143:608–31. https://doi.org/10.1016/j.watres.2018.07.029.
9. Bolto B, Gregory J. Organic polyelectrolytes in water treatment. Water Res. 2007;41:2301–24. https://doi.org/10.1016/j.watres.2007.03.012.
10. Abbasi Moud A. Polymer based flocculants: review of water purification applications. J Water Process Eng. 2022;48:102938. https://doi.org/10.1016/j.jwpe.2022.102938.
11. Zinatizadeh AA, Ibrahim S, Aghamohammadi N, Mohamed AR, Zangeneh H, Mohammadi P. Polyacrylamide-induced coagulation process removing suspended solids from palm oil mill effluent. Separat Sci Technol. 2017;52:520–7. https://doi.org/10.1080/01496395.2016.1260589.
12. Bhatia S, Othman Z, Ahmad AL. Pretreatment of palm oil mill effluent (POME) using Moringa oleifera seeds as natural coagulant. J Hazard Mater. 2007;145:120–6. https://doi.org/10.1016/j.jhazmat.2006.11.003.
13. Zhou J, Li H, Zhang X. Synergy between dual polymers and sand-to-fines ratio for enhanced flocculation of oil sand mature fine tailings. Energy Fuels. 2021;35:8884–94. https://doi.org/10.1021/acs.energyfuels.1c00620.
14. Morris KF, Johnson CS. Diffusion-ordered two-dimensional nuclear magnetic resonance spectroscopy. J Am Chem Soc. 1992;114:3139–41. https://www.semanticscholar.org/paper/Diffusion-ordered-two-dimensional-nuclear-magnetic-Morris-Johnson/692e726e81d99c80b1864eb015cb85cb64aace19.
15. Morris KF, Johnson CS. Resolution of discrete and continuous molecular size distributions by means of diffusion-ordered 2D NMR spectroscopy. J Am Chem Soc. 1993;115:4291–9. https://doi.org/10.1021/ja00063a053.
16. Johnson CS. Diffusion ordered nuclear magnetic resonance spectroscopy: principles and applications. Prog Nucl Magn Reson Spectrosc. 1999;34:203–56. https://doi.org/10.1016/S0079-6565(99)00003-5.
17. Claridge TDW Chapter 10 - Diffusion NMR spectroscopy. In: Claridge TDW, editor. High-resolution NMR techniques in organic Chemistry (Third Edition). Boston: Elsevier; 2016. p. 381–419.
18. Chen A, Wu D, Johnson CSJ. Determination of molecular weight distributions for polymers by diffusion-ordered NMR. J Am Chem Soc. 1995;117:7965–70.
19. Lodge TP. Reconciliation of the molecular weight dependence of diffusion and viscosity in entangled polymers. Phys Rev Lett. 1999;83:3218–21. https://doi.org/10.1103/PhysRevLett.83.3218.
20. Håkansson B, Nydén M, Söderman O. The influence of polymer molecular-weight distributions on pulsed field gradient nuclear magnetic resonance self-diffusion experiments. Colloid Polym Sci. 2000;278:399–405. https://doi.org/10.1007/s003960050532.
21. Kanematsu T, Sato T, Imai Y, Ute K, Kitayama T. Mutual- and self-diffusion coefficients of a semiflexible polymer in solution. Polym J. 2005;37:65–73. https://doi.org/10.1295/polymj.37.65.
22. Xu M, Xu M, Chen Q, Zhang S. Investigation on extremely dilute solution of PEO by PFG-NMR. Colloid Polym Sci. 2009;288:85. https://doi.org/10.1007/s00396-009-2146-5.
23. Vieville J, Tanty M, Delsuc MA. Polydispersity index of polymers revealed by DOSY NMR. J Magn Reson. 2011;212:169–73. https://doi.org/10.1016/j.jmr.2011.06.020.
24. Li W, Chung H, Daeffler C, Johnson JA, Grubbs RH. Application of 1H DOSY for facile measurement of polymer molecular weights. Macromolecules. 2012;45:9595–603. https://doi.org/10.1021/ma301666x.
25. Lewinski P, Sosnowski S, Kazmierska S, Penczeka S. L-Lactide polymerization studied by 1H NMR with diffusion-ordered spectroscopy (DOSY): a "One NMR Tube Experiment" providing data

on monomer conversion, polymer structure, Mn and Mw. Polym Chem. 2015;6:4353–7. https://doi.org/10.1039/x0xx00000x.
26. Arrabal-Campos FM, Oña-Burgos P, Fernández I. Molecular weight prediction with no dependence on solvent viscosity. A quantitative pulse field gradient diffusion NMR approach. Polym Chem. 2016;7:4326–9. https://doi.org/10.1039/C6PY00691D.
27. Chamignon C, Duret D, Charreyre M-T, Favier A. 1H DOSY NMR determination of the molecular weight and the solution properties of poly(N-acryloylmorpholine) in Various Solvents. Macromol Chem Phys. 2016;217:2286–93. https://doi.org/10.1002/macp.201600089.
28. Guo X, Laryea E, Wilhelm M, Luy B, Nirschl H, Guthausen G. Diffusion in polymer solutions: molecular weight distribution by PFG-NMR and relation to SEC. Macromol Chem Phys. 2017;218. https://doi.org/10.1002/macp.201600440.
29. Rosenboom J-G, De Roo J, Storti G, Morbidelli M Diffusion (DOSY) 1H NMR as an alternative method for molecular weight determination of poly(ethylene furanoate) (PEF) polyesters. Macromol Chem Phys. 2017;218. https://doi.org/10.1002/macp.201600436.
30. Gu K, Onorato J, Xiao SS, Luscombe CK, Loo Y-L. Determination of the molecular weight of conjugated polymers with diffusion-ordered NMR spectroscopy. Chem Mater. 2018;30:570–6. https://doi.org/10.1021/acs.chemmater.7b05063.
31. Nam NH, Tho NH, Ngoc NM, Trung PQ. Application of 1H DOSY NMR in measurement of polystyrene molecular weights. VNU J Sci: Natural Sci Technol. 2020;36. https://doi.org/10.25073/2588-1140/vnunst.4917.
32. Hou J, Pearce E. Characterization of polymer molecular weight distribution by NMR diffusometry: experimental criteria and findings. Anal Chem. 2021;93:7958–64. https://doi.org/10.1021/acs.analchem.1c00793.
33. Grabe B, Hiller W. Molar mass distribution and chemical composition distribution of PS-b-PMMA block copolymers determined by diffusion ordered spectroscopy. Macromolecules. 2022;55:8014–20. https://doi.org/10.1021/acs.macromol.2c01505.
34. Voorter P-J, McKay A, Dai J, Paravagna O, Cameron NR, Junkers T. Solvent-independent molecular weight determination of polymers based on a truly universal calibration. Angewandte Chemie Int Ed. 2022;61:e202114536. https://doi.org/10.1002/anie.202114536.
35. Jerschow A, Müller N. Diffusion-separated nuclear magnetic resonance spectroscopy of polymer mixtures. Macromolecules. 1998;31:6573–8.
36. Van Gorkom LCM, Hancewicz TM. Analysis of DOSY and GPC-NMR experiments on polymers by multivariate curve resolution. J Magn Reson. 1998;130:125–30.
37. Ute K, Nagao R, Watanabe K. Application of on-line SEC-NMR and DOSY for practical polymer characterization. In: Zhang R, Miyoshi T, Sun P, editors. NMR Methods for Characterization of Synthetic and Natural Polymers. New Developments in NMR. Cambridge: The Royal Society of Chemistry; 2019. p. 80–100.
38. Barrère C, Mazarin M, Giordanengo R, Phan TNT, Thévand A, Viel S, et al. Molecular weight determination of block copolymers by pulsed gradient spin echo NMR. Anal Chem. 2009;81:8054–60. https://doi.org/10.1021/ac9018654.
39. Viel S, Mazarin M, Giordanengo R, Phan TN, Charles L, Caldarelli S, et al. Improved compositional analysis of block copolymers using diffusion ordered NMR spectroscopy. Anal Chim Acta. 2009;654:45–8. https://doi.org/10.1016/j.aca.2009.06.049.
40. Natalello A, Alkan A, Friedel A, Lieberwirth I, Frey H, Wurm FR. Enlarging the toolbox: epoxide termination of polyferrocenylsilane (PFS) as a key step for the synthesis of amphiphilic PFS–polyether block copolymers. ACS Macro Lett. 2013;2:313–6. https://doi.org/10.1021/mz400080s.
41. Hiller W. Quantitative studies of block copolymers and their containing homopolymer components by diffusion ordered spectroscopy. Macromol Chem Phys. 2019;220:1900255. https://doi.org/10.1002/macp.201900255.
42. Chang BS, Ma L, He M, Xu T. NMR studies of block copolymer-based supramolecules in solution. ACS Macro Lett. 2020;9:1060–6. https://doi.org/10.1021/acsmacrolett.0c00434.
43. Xu J, Wang X, Hadjichristidis N. Diblock dialternating terpolymers by one-step/one-pot highly selective organocatalytic multimonomer polymerization. Nat. Commun. 2021;12:7124. https://doi.org/10.1038/s41467-021-27377-3.
44. Groves P. Diffusion ordered spectroscopy (DOSY) as applied to polymers. Polym Chem. 2017;8:6700–8. https://doi.org/10.1039/C7PY01577A.
45. Wu D, Chen A, Johnson CS Jr. An improved diffusion-ordered spectroscopy experiment incorporating bipolar-gradient pulses. J Magnet Reson Series A. 1995;115:260–4.
46. Watanabe K, Ute K. Characterization of high molecular weight acrylamide-based copolymers by DOSY-NMR using high field-gradients. Kobunshi Ronbunshu. 2018;75:358–62. https://doi.org/10.1295/koron.2018-0005.
47. Lopez CG, Linders J, Mayer C, Richtering W. Diffusion and viscosity of unentangled polyelectrolytes. Macromolecules. 2021;54:8088–103. https://doi.org/10.1021/acs.macromol.1c01169.
48. Provencher SW. CONTIN: a general purpose constrained regularization program for inverting noisy linear algebraic and integral equations. Comput Phys Commun. 1982;27:229–42. https://doi.org/10.1016/0010-4655(82)90174-6.
49. Provencher SW. A constrained regularization method for inverting data represented by linear algebraic or integral equations. Comput Phys Commun. 1982;27:213–27. https://doi.org/10.1016/0010-4655(82)90173-4.
50. Wang J, Huang H, Huang X. Molecular weight and the Mark-Houwink relation for ultra-high molecular weight charged polyacrylamide determined using automatic batch mode multi-angle light scattering. J Appl Polym Sci. 2016;133. https://doi.org/10.1002/app.43748.
51. De Gennes PG. Dynamics of entangled polymer solutions. I. The Rouse Model. Macromolecules. 1976;9:587–93. https://doi.org/10.1021/ma60052a011.
52. Colby RH. Structure and linear viscoelasticity of flexible polymer solutions: comparison of polyelectrolyte and neutral polymer solutions. Rheologica Acta. 2010;49:425–42. https://doi.org/10.1007/s00397-009-0413-5.
53. Prabhu VM, Muthukumar M, Wignall GD, Melnichenko YB. Polyelectrolyte chain dimensions and concentration fluctuations near phase boundaries. J Chem Phys. 2003;119:4085–98. https://doi.org/10.1063/1.1592496.
54. Caizán-Juanarena L, ter Heijne A, Weijma J, Yntema D, Suárez-Zuluaga DA, Buisman CJN. Screening for electrical conductivity in anaerobic granular sludge from full-scale wastewater treatment reactors. Biochem Eng J. 2020;159:107575. https://doi.org/10.1016/j.bej.2020.107575.
55. Hyrycz M, Ochowiak M, Krupińska A, Włodarczak S, Matuszak M. A review of flocculants as an efficient method for increasing the efficiency of municipal sludge dewatering: mechanisms, performances, influencing factors and perspectives. Sci Total Environ. 2022;820:153328. https://doi.org/10.1016/j.scitotenv.2022.153328.
56. Zhang X, Ye P, Wu Y. Enhanced technology for sewage sludge advanced dewatering from an engineering practice perspective: a review. J Environ Manag. 2022;321:115938. https://doi.org/10.1016/j.jenvman.2022.115938.